LA-4843

C.3

Effect of Target Thermal Conductivity and Roughness on the Initiation of PBX 9404 by Oblique Impact

los alamos
scientific laboratory
of the University of California
LOS ALAMOS, NEW MEXICO 87544

UNITED STATES
ATOMIC ENERGY COMMISSION
CONTRACT W-7405-ENG. 36

Printed in the United States of America. Available from
National Technical Information Service
U. S. Department of Commerce
5285 Port Royal Road
Springfield, Virginia 22151
Price: Printed Copy $3.00; Microfiche $0.95

LA-4843
UC-34
ISSUED: March 1972

Effect of Target Thermal Conductivity and Roughness on the Initiation of PBX 9404 by Oblique Impact

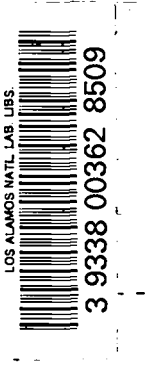

by

Alan D. Randolph
L. E. Hatler
A. Popolato

EFFECT OF TARGET THERMAL CONDUCTIVITY AND ROUGHNESS ON THE INITIATION OF PBX 9404 BY OBLIQUE IMPACT

by

Alan D. Randolph, L. E. Hatler, and A. Popolato

ABSTRACT

The effect of target thermal conductivity and surface roughness on the drop heights required to initiate a reaction in pressed hemispherical billets of PBX 9404 subjected to oblique impact was evaluated. In a first series of tests, the explosive struck targets of fused quartz, aluminum oxide, and gold with similar surface characteristics. The experimentally determined estimates of the drop heights required to produce an explosion ranged over two orders of magnitude, with the high-conductivity gold target and the low-conductivity quartz target being, respectively, the least and most sensitive. The effect of surface roughness on drop height was evaluated in a second series of drops onto fused-quartz targets with differing surface finishes. The results from both tests were satisfactorily reproduced by computer simulation of the mechanical and thermal events occurring during the oblique-impact loading of the charge to ignition. No attempt was made to calculate the buildup from ignition to detonation. Concentrations of energy, i.e., thermal "hot spots," were found to be unnecessary to satisfactorily explain the experimental observations.

NOMENCLATURE

a	radius of deformation circle on HE billet, cm	g	gravitational acceleration constant, $(g_f\text{-cm})/(g_m\text{-sec}^2)$
a'	a trigonometric term relating billet diameter to the tangential force moment arm	H	vertical drop height, cm or ft
A	area of contact deformation circle on HE billet, cm^2	ΔH	heat of reaction (burning) for HE, cal/g
b'	a trigonometric term relating billet diameter to the normal force moment arm	I	moment of inertia of billet, $cm^2\text{-g}$
c	specific heat of HE, cal/g-°C	J	conversion factor from mechanical to thermal units
D	diameter of HE billet, cm	k	thermal conductivity, cal/sec-cm-°R
d	deformation diameter on HE billet, cm	K	constant relating d_c to $H^{1/4}$
E	activation energy, kcal/mol	M. W.	molecular weight of HE, g/g-mol
F	force acting on billet, dyn	M	rotational moments due to contact forces, dyn-cm

q	thermal flux generated at billet-target interface, cal/cm^2-sec
R	radius of hemisphere, cm or in.
r	HE reaction (burning) rate, mol/sec-cm^3
t	time, sec
T	temperature of billet, °K
V	billet velocity, cm/sec
W	weight of billet, g or lb
X	deformation of billet normal to impact target, cm
X'	moment arm about HE center of gravity for tangential force, cm
X''	moment arm about HE center of gravity for normal force, cm
X'''	distance from HE center of gravity to center of contact circle, cm
Y	distance coordinate of HE center of gravity parallel to impact target, cm
y	fraction of HE reacted
Z	frequency factor, sec^{-1}
α	thermal diffusivity, cm^2/sec
γ	tangential shear stress, dyn/cm^2
$\dot{\theta}$	angular velocity of hemisphere billet after rebound, rad/sec
μ	coefficient of sliding friction
θ	angle with horizontal of diameter of hemisphere billet after rebound, rad
ρ	HE density, g/cm^3
σ	normal plastic flow stress, dyn/cm^2
φ	angle of target plane to horizontal for vertical drop, or complement of angle of approach for pendulum drop, degrees
ψ	angle of target plane to horizontal for vertical drop, or angle of billet tip from horizontal in pendulum configuration, degrees, maintained approximately zero
ω	angular velocity, rad/sec

Subscripts

B	relating to boundary conditions
c	relating to maximum deformed area on HE billet and contact time
x	forces or motions in x-direction
y	forces or motions in y-direction
cg	motions or moment of inertia about center of gravity
n	normal to target
τ	tangential to target
1	refers to properties of the HE
2	refers to properties of the target

Superscripts

o	relating to initial conditions at instant of impact
$\cdot$	a dot above a symbol represents the derivative with respect to time
$\cdot\cdot$	two dots above a symbol represents the second derivative with respect to time

I. INTRODUCTION

Large, uncased billets of secondary high explosives such as the cast cyclotols (mixtures of 2, 4, 6-trinitrotoluene and hexahydro-1, 3, 5-trinitro-s-triazine) and plastic-bonded explosives containing RDX (hexahydro-1, 3, 5-trinitro-s-triazine) or HMX (octahydro-1, 3, 5, 7-tetranitro-1, 3, 5, 7-tetrazocine) are quite stable during normal impact on smooth surfaces. Impact velocities of about 100 ft/sec are generally required to initiate a reaction (violent deflagration or detonation) in void-free, high-density billets. With an oblique impact, such as sliding or skidding, these explosives can be initiated at impact velocities of about 10 ft/sec. Serious handling accidents have occurred in which it was theorized that the HE was initiated in this way. Such initiations suggest a thermal mechanism of initiation in which transformation of mechanical to thermal energy initiates a thermal decomposition reaction that grows to violent deflagration or detonation under proper conditions of confinement and mass of HE. Large PBX 9404 charges typically build to violent explosion, sometimes approaching high-order detonation.

Several skid tests have been devised to study initiation by oblique impact. Such tests have been used to assess the handling safety characteristics of bare explosive billets. Dyer and Taylor[1] describe an oblique-impact test in which a hemispherical billet of HE is suspended in a harness with its flat surface held horizontal. The billet swings down on the end of the harness and strikes

against a rigid horizontal target at a predetermined angle. The test variables are the drop height, the angle of impact between the billet and target, and the surface condition and composition of the target. A schematic of this skid test configuration, which we will call the pendulum drop configuration, is shown in Fig. 1.

We have developed a similar skid test in which hemispherical billets are dropped in free fall against an inclined rigid target. A schematic of this drop configuration, which we will call the vertical drop configuration, is shown in Fig. 2.

With either version of the skid test, violent reactions can occur from much lower drop heights than would be necessary to initiate a reaction with normal impact.

A better understanding of the skid test is important in assessing the hazards associated with handling large billets of high explosives. This report gives the results of work that conclusively demonstrates that the mechanism of initiation in an oblique impact against a relatively smooth target surface is thermal generation and transport at the target-billet interface. Experimental results obtained when both the thermal-transport properties and surface finish of the target were varied can be explained by straightforward mechanical and thermal calculations of this uniform flux without

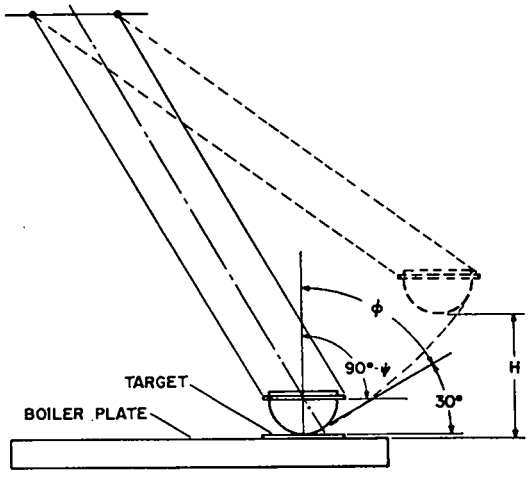

Fig. 1. Pendulum drop configuration.

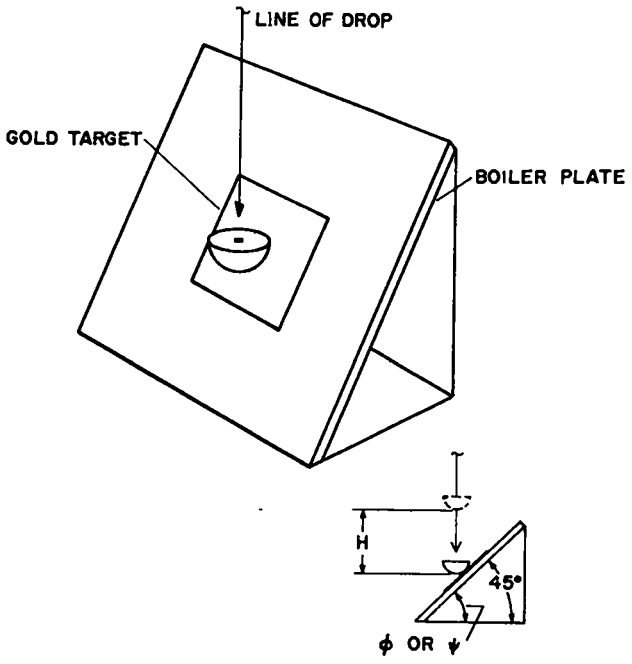

Fig. 2. Vertical drop configuration.

assuming localized concentrations of thermal energy as in Bowden's hot-spot theory of initiation.[2]

Bowden and Gurton,[2] in a classic study of HE initiation, demonstrated that the thermal-transport mechanisms play a dominant role in the impact initiation of secondary explosives. The "sensitization" of HE by grit particles in both friction and impact sensitivity tests was attributed to initiation at thermal hot spots, where the grit particles developed high temperatures at points of grit-grit or grit-HE contact. Yoffe[3] used this thermal-transport theory of initiation to explain the initiation of HE by adiabatic compression of entrapped gas in a hammer-anvil sensitivity apparatus.

In the skid test, the thermal-transport theory suggests that the primary mechanism of initiation is thermal generation and transport at the billet-target interface. Thermal generation is determined by the sliding velocity, surface roughness, and mechanical properties of the billet; thermal transport is influenced by the thermal diffusivities of billet and target.

Definitive answers to the questions of thermal generation and transport at sliding unlubricated surfaces are not available. Furey[4], in a recent review article on friction and lubrication, states that "we know practically nothing about the magnitude and distribution of surface temperatures in real systems." Holm[5] presented a theoretical study of transient temperature rise in a sliding circular contact, based on simplifications of earlier work by Jaeger. Average temperatures at the sliding interface were deduced by measuring the thermocouple emf generated at the bimetallic surface. Fair agreement was obtained between theoretical and experimental results, but numerous simplifications were used in estimating the thermal flux generated at the surface. Archard[6] presented a comprehensive theoretical study of the temperature of rubbing surfaces. Small localized circular points of true contact between the two materials were assumed, and the highest transient temperatures developed at these localized points of contact were calculated. Two limiting cases, high and low sliding velocity, were considered. In the former case, a small contact sees a stationary unheated surface at the boundary, whereas in the latter case, temperatures have time to accommodate to steady profiles on both sides of the interface. In both cases, the total thermal flux was partitioned between the two surfaces so that the appropriate equations for heat flow in the two media gave the same surface temperature.

In the present study, thermal generation and transport at the billet-target surface were described by considering the total measurable contact area between the deformed billet and rigid target as the true contact area. Thus, no concentration of energy due to localized contact was assumed. Thermal flux was calculated from the work done at the sliding surface by direct measurement of tangential forces. These forces were expressed in terms of an apparent coefficient of sliding friction defined as the ratio of tangential to normal contact forces.

The deformed area on the billet is much greater than the additional area covered by sliding displacement during contact. Physically, this corresponds to the low-velocity case described by Holm.

A necessary consequence of applying the thermal-transport theory of initiation to the skid test is that thermal diffusivities in both explosive and target, as well as surface roughness of the target, should play an important role in determining HE response. This thermal-transport theory of initiation was first tested by a series of oblique impacts of hemispherical billets of PBX 9404[plastic-bonded explosive composed of 94 wt % HMX, 3 wt % nitrocellulose, and 3 wt % tris-(beta chloroethyl) phosphate] on three smooth target surfaces having widely divergent thermal diffusivities. These target surfaces were fused quartz, aluminum oxide, and gold. In a second series of tests, PBX 9404 hemispherical billets struck fused quartz targets having different surface finishes. In both series of drops, the time-dependent thermal flux generated at the target-billet interface was calculated from measurements of billet impact dynamics, and these fluxes were used in a numerical analysis of the mechanical-thermal dynamics. Experimental data were adequately explained by this computer simulation.

II. ANALYSIS OF SKID TEST

A. Billet Dynamics

The heat flux generated at the sliding billet target interface is calculated as

$$q = \mu \sigma V_T / J \quad \text{cal/sec-cm}^2, \qquad (1)$$

where μ is an apparent coefficient of friction equal to the ratio of tangential to normal contact forces, σ is the normal contact pressure (in this case equal to the plastic-flow stress of the explosive), V_T is the sliding velocity, and J is the conversion factor from mechanical to thermal units. This heat flux occurs over the contact area A(t) during the contact time t_c. Thus, analysis of thermal transport in the skid test must begin with an analysis of impact dynamics. The three pertinent equations of

motion for the center of mass of an impacting plastic hemisphere on a rigid plane surface can be written as

$$W\ddot{X} = F_x, \quad (2)$$

$$W\ddot{Y} = F_y, \quad (3)$$

and

$$I_{cg}\ddot{\theta} = M_{cg}. \quad (4)$$

B. Analysis of Normal Motion

If functional relationships between force and normal deformation are known, Eqs. (2) through (4) can be integrated with the initial conditions defined at the instant of impact. The solution yields the normal deformation-time and velocity-time profiles during impact. Trigonometry relates the hemisphere diameter D, radius of deformation a, and normal deformation X (for small deformations) as

$$a^2 \doteq DX.$$

The deformed area is then related to the normal deformation as

$$A(t) = \pi a^2 = \pi DX.$$

If the stress-strain relation for the hemisphere is assumed to be that of constant normal stress, i.e., plastic flow at the plastic-flow stress σ, then the normal force is given as

$$F_x = \sigma \pi DX.$$

Equation (2) has the solution

$$X = (V_n^o/\omega) \sin \omega t,$$

for $0 \leq t \leq \pi/2\omega$ and where

$$\omega = (\pi \sigma D/W)^{1/2}.$$

The normal velocity during impact is given as

$$V_n = \dot{X} = V_n^o \cos \omega t.$$

At $\omega t_c = \pi/2$, V_n is zero and the hemisphere has come to rest, giving the contact time during impact as

$$t_c = \pi/2\omega = (\pi/2)(W/\pi \sigma D)^{1/2}.$$

This contact time is independent of impact velocity V_n^o and varies with $\sigma^{-1/2}$. The impact is assumed to be plastic, so weak forces during rebound are neglected in the analysis of motion. The maximum contact area is given by

$$A_c = \pi DV_n^o/\omega.$$

If the hemisphere is dropped a vertical distance H (see Fig. 2) on a target plate inclined at an angle φ with the horizontal, the normal impact velocity is given as

$$V_n^o = (2gH)^{1/2} \cos \varphi.$$

For the pendulum drop (Fig. 1), the angle φ is taken as the complement of the angle of approach to the horizontal target. The drop height and maximum deformed area are related as

$$A_c = (\pi D/\omega)(2gH)^{1/2} \cos \varphi,$$

but

$$A_c = \pi d_c^2/4,$$

where d_c is maximum contact deformation diameter. Thus, the relationship between drop height and maximum deformation diameter is given by

$$d_c^4 = (32DWg \cos^2 \varphi/\pi \sigma)H, \quad (5)$$

or

$$d_c = KH^{1/4}, \quad (6)$$

where K is a constant that depends on drop angle and physical properties. Equation (6) provides a simple way of verifying the constant-stress impact model as well as determining quantitative values for the normal plastic-flow stress σ under actual drop conditions (Fig. 3).

C. Analysis of Rotational Motion

Equation (4) for rotation about the center of gravity can be solved with initial conditions $\theta(0) = 0$ and $\dot{\theta}(0) = 0$ to predict the rotational velocity of the billet about its center of gravity. The moments about the center of gravity of a hemisphere are given by

$$M_{cg} = X''F_n + X'F_\tau,$$

where

$$X' = R(1 - 0.375 \cos \psi),$$

$$X'' = 0.375R \sin \psi,$$

and ψ is the angle of the target with the horizontal. Note: $\psi = \varphi$ for vertical drops when the flat surface of the hemisphere is horizontal at impact (Figs. 1 and 2). With regard to rotation, the pendulum and vertical drop tests are fundamentally different.

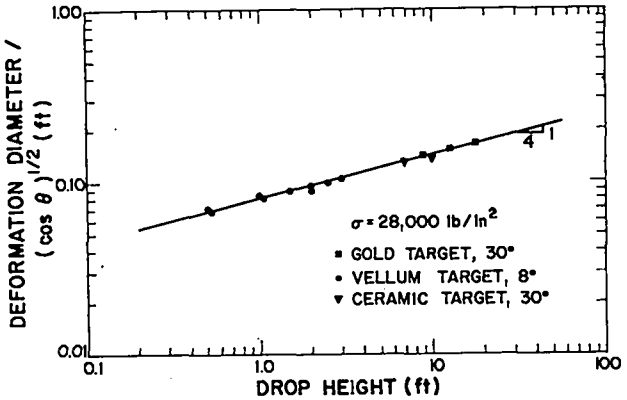

Fig. 3. Relation of deformation diameter to drop height.

Because the harness in the pendulum drop test always keeps the hemisphere horizontal, the angle ψ is always zero, and the component of normal force passes through the center of gravity, with no contribution to rotational motion. Normal and tangential forces are given in terms of the deformed area and normal and tangential stresses as

$$F_n = \sigma \pi a^2,$$

and

$$F_T = \gamma \pi a^2,$$

where, again,

$$a^2 = DX,$$

from the preceding analysis of normal motion. Thus, the differential equation for angular rotation is

$$\ddot{\theta} = \left[(a'\mu + b')\pi D^2 V_n^o \sigma / 2I_{cg}\omega\right] \sin \omega t,$$

with initial conditions $\theta(0) = 0$, $\dot{\theta}(0) = 0$, and with

$$a' = 1 - 0.375 \cos \psi,$$

$$b' = 0.375 \sin \psi.$$

For the pendulum configuration, with the billet top in a horizontal plane, b' equals 0 and only the tangential forces contribute to rotation. The apparent coefficient of sliding friction,

$$\mu = \gamma/\sigma,$$

is given as the ratio of tangential to normal stresses. Using only the second initial condition to solve for angular velocity during impact gives

$$\dot{\theta} = \left[(a'\mu + b')\pi D^2 V_n^o \sigma / 2I_{cg}\omega^2\right](1 - \cos \omega t). \quad (7)$$

Because

$$\omega^2 = \pi D \sigma / W,$$

Eq. (7) becomes

$$\dot{\theta} = \left[(a'\mu + b')DV_n^o W / 2I_{cg}\right](1 - \cos \omega t).$$

At the end of the impact time, $\omega t_c = \pi/2$. The final angular velocity imparted to the hemisphere (again neglecting friction during rebound) is thus given as

$$\dot{\theta}_c = (a'\mu + b')DV_n^o W / 2I_{cg}. \quad (8)$$

For a hemisphere,

$$I_{cg}/W = 0.0648D^2$$

Thus, angular rotation after rebound is given as

$$\dot{\theta}_c = 7.72\,(a'\mu + b')V_n^o / D.$$

Alternatively, the apparent coefficient of friction can be obtained in terms of drop velocity, diameter, and angular velocity after rebound as

$$\gamma/\sigma = \mu = (1/a')(0.13\,D\dot{\theta}_c / V_n^o - b'). \quad (9)$$

Equation (9) suggests that tangential stress γ can be obtained by measuring the constant final angular velocity in the period of free rotation after rebound with the aid of a high-speed motion picture.

D. Analysis of Tangential Motion

The equation for translation of the center of gravity of the impacting billet in a direction parallel to the target surface, i.e., tangential motion, can be obtained by the integration of Eq. (3) subject to the initial conditions

$$Y(0) = 0,$$

and

$$\dot{Y}(0) = V_T^o = V^o \sin \varphi,$$

where, again, φ is the complement of the angle of approach for the pendulum configuration or is the target angle ψ for the vertical-drop configuration. The tangential force is given as

$$F_T = -\gamma \pi DX.$$

Substituting for $X(t)$ and replacing γ and $\mu\sigma$ gives

$$\ddot{Y} = -(\mu \sigma \pi DV^o \cos \varphi / \omega W) \sin \omega t.$$

Using only the second initial condition to obtain Y, the tangential velocity of the center of gravity, gives

$$\dot{Y} = (V_T)_{cg} = V^o \left[\sin \varphi + \mu \cos \varphi (\cos \omega t - 1)\right].$$

Finally, the sliding velocity along the target surface can be obtained by correcting for rotation:

$$V = (V_T)_{cg} - X'''\dot{\theta},$$

where

$$X''' = \left[(X')^2 + (X'')^2\right]^{1/2}.$$

Correcting for rotation as derived in Eq. (8) gives the final value for tangential velocity as

$$V_T/V^0 = \sin\varphi - \left[\mu + (a'\mu + b')\, DWX'''/2I_{cg}\right] \cos\varphi\,(1 - \cos\omega t). \qquad (10)$$

E. Thermal Transients at Billet-Target Interface

The preceding analysis of mechanical-impact dynamics permits a quantitative evaluation of thermal flux generated at the billet-target interface from calculated motions of the impacting billet. Heat flux generated on the surface is equal to the rate of work done at the surface expressed in thermal units. In the calculation of the heat flux from Eq. (1), V_T is given by Eq. (10); μ and σ are obtained by analysis of impact motion using Eqs. (9) and (5). Equation (1), partitioned between billet and target, provides a time-dependent boundary condition to the reactive heat-transfer equation. The use of Eq. (1) as a boundary condition is equivalent to assuming that all the frictional work is generated as a line source between the two sliding surfaces, rather than as viscous dissipation in the flowing plastic.

The one-dimensional heat equation in two media, with the reaction term present for HE, was solved with the flux partitioned between the billet and target according to Fourier's law written at each instant of time. The one-dimensional heat equation is stated for HE[7] and target as

$$\frac{\partial T_1}{\partial t} = \alpha_1 \frac{\partial^2 T_1}{\partial x^2} + (1 - y)\Delta H r/\rho c, \qquad (11)$$

and

$$\frac{\partial T_2}{\partial t} = \alpha_2 \frac{\partial^2 T_2}{\partial X^2}, \qquad (12)$$

where the subscripts 1 and 2 refer to the HE and the target, respectively. ΔH and r are the heat of reaction (burning) and the rate for the HE, and y is the fraction reacted,* which is given by

$$y = (M.W./\rho)\int_0^t r\,dt. \qquad (13)$$

The reaction rate, r, for PBX 9404 can be adequately represented by Arrhenius-type reaction rate kinetics of the form

$$Z \exp\left[-E/RT\right].$$

The boundary conditions used for solution of Eqs. (11) and (12) are continuity of temperature at the billet-target interface,

$$T_1(0,t) = T_2(0,t) = T_s(t), \qquad (14)$$

and a partitioning of flux as given by Fourier's law,

$$q(t) = \left|q_1\right| + \left|q_2\right| = k_1\left|\frac{\partial T_1(0,t)}{\partial x}\right| + k_2\left|\frac{\partial T_2(0,t)}{\partial x}\right|. \qquad (15)$$

Boundary conditions (14) and (15) are expressed numerically as

$$T_s(t) = \left[\Delta x_1 \Delta x_2/(k_1\Delta x_2 + k_2\Delta x_1)\right] q(t) + \left[k_1\Delta x_2/(k_1\Delta x_2 + k_2\Delta x_1)\right] T_1^{(1)} + \left[k_2\Delta x_1/(k_1\Delta x_2 + k_2\Delta x_1)\right] T_2^{(1)}, \qquad (16)$$

where T_s is a hypothetical boundary temperature and $T^{(1)}$ is the first computational mesh temperature in billet or target.

Equations (11), (12), and (13) were finite-differenced with an explicit forward difference scheme and, together with Eq. (16), were made dimensionless for efficient digital computation. Computations were carried out on LASL's CDC-6600 computer. Each separate run simulates

* Because of the critical behavior of the reaction term for secondary explosives (E typically 45 to 55 kcal/mol), no appreciable error in calculating explosion time is caused by neglecting the fraction of HE reacted. Equation (13) is merely added to complete the formalism and as a computational convenience to define the point of thermal explosion.

thermal phenomena after impact from a vertical height H. Three normal exits from the program are provided: "thermal event," "hemisphere rebounds," or "hemisphere stops sliding." A "thermal event" occurs when the fraction reacted exceeds the value 0.99 at any computational mesh point. The critical height to develop a thermal event is found by direct search of the height space between upper and lower bounds. The search algorithm chooses the next height for evaluation as the geometric mean of the lowest "go" and highest "no go" heights, thus converging in 12 to 15 calculations to the true critical height.

III. EXPERIMENTAL APPARATUS AND PROCEDURE

In a first series of drops, hemispherical billets of PBX 9404 struck rigid targets of fused quartz, aluminum oxide, and gold to determine the effect of the thermal conductivity of the targets on the 50% drop height.*

Each 10-in.-diam billet is composed of a small, 7.5-lb inner hemisphere of inert material, with an 11-lb outer shell of PBX 9404 glued to it. A 0.5-in.-diam Micarta plate is glued to the top of the billet for attachment to the drop apparatus. Total weight of the assembly is 19.1 lb. Figure 4 shows the assembly of the components of the billets.

Two drop configurations were used to strike the billets against the targets. A pendulum drop configuration (Fig. 1) was used to strike the PBX 9404 against the quartz and aluminum oxide targets. This configuration was chosen because a 6-in.-square target could be hit consistently. The angle

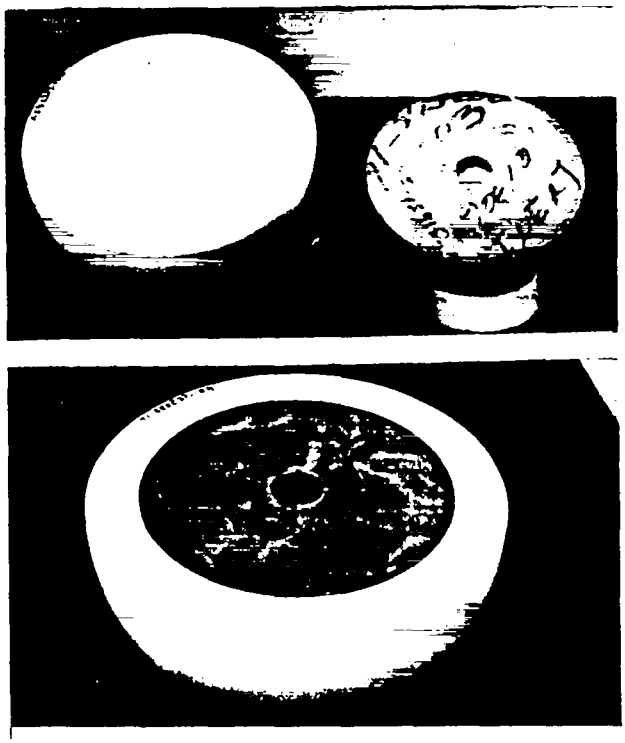

Fig. 4. Hemispherical drop test billet.

of impact was 30° to the horizontal target. The pendulum configuration had a vertical limitation of 20 ft, so a vertical drop configuration (Fig. 2) was used for the gold target experiments. The impact angle was 45°. In both configurations, the targets were rigidly secured to a 4-in.-thick steel boiler plate.

The fused-quartz targets were 6 in. square by 0.25 in. thick. Their surfaces were ground with an intermediate grit on a grinding wheel to give a roughness of 50 to 80 μin. as measured by a Cutler Hammer Surf-Indicator. The targets were attached to the 4-in.-thick steel boiler plate with epoxy adhesive.

The 10 by 10 by 0.25-in. aluminum oxide targets were purchased from Coors Ceramics and were nominally 85% alumina and 15% silica, magnesia, and calcia. Three of these targets were ground with boron carbide to give a surface roughness of 50 to 80 μin., and nine others were ground with aluminum oxide to give a surface roughness of

* The height at which there is a 50-50 chance, statistically calculated, that an explosive event will occur. The statistics in the "up-down" testing and analysis procedure assume that the probabilities for an explosive event are distributed log-normally about the median height. Thus, the "50% drop height" is, in fact, the estimated median height where the probability for an event is one-half.[8]

20 to 35 μin. These ceramic targets were rigidly mounted with epoxy adhesive to the 4-in.-thick steel boiler plate.

The gold targets were prepared by electroplating a 7-mil-thick layer of copper on a sheet of Dural, 10 in. square and 0.25 in. thick. A 3-mil layer of gold was then electroplated on the copper and polished to a surface roughness of 50 to 80 μin. Four of these 10-in. targets were mounted with epoxy adhesive on a sheet of aluminum as a 20-in.-square target. This target was then bolted to the 4-in.-thick steel boiler plate.

The apparent coefficients of friction and the plastic-flow stress in the billet were determined experimentally in both the first and second series of drops for use in the mechanical-thermal initiation calculations. High-speed motion pictures of the "no go" impacts were analyzed to determine the tangential forces under the conditions of impact. The angular velocity after rebound was found by plotting the change in angle of the HE billet as a function of time. The angular velocity imparted to the billet during contact is expressed in terms of contact stress, moment of inertia, geometry, and ratio of tangential to normal forces (apparent coefficient of friction) in Eq. (8). This relationship was used to calculate the apparent coefficient of friction from the measured angular velocity, together with the geometrical and mechanical properties of the billet. Measured apparent coefficients of friction were about 0.1 for the targets used in the first series of drops, and varied from 0.06 to 0.24 in the second drop series.

Plastic-flow stress was determined by dropping PBX-9404 billets vertically onto an 8° inclined boiler plate target covered by a sheet of vellum backed with carbon paper. Drop heights ranged from 5 to 36 in. The maximum circle of deformation on the billet at impact could be measured accurately from the circle imprinted on the vellum by the carbon paper. From the deformation diameter, weight and diameter of the billet, and the target angle, the plastic-flow stress in the billet was determined from Eq. (5). Reproducible values of the plastic-flow stress calculated for different drop heights verified that the billets struck with constant stress and plastic flow (Fig. 3). The permanently deformed area on the billets after impact was found to be 85 to 90% of the maximum deformed area (measured by the carbon paper imprint); therefore, normal forces during rebound were neglected in the idealized impact model used in thermal calculations.

The apparatus indicating vertical drop height was calibrated for both pendulum and vertical drops. Thermal events were verified by detailed examination of high-speed motion pictures of each drop; overpressures were measured for some drops.

The experimental results from this first series of drops on surfaces of different thermal conductivity indicated that surface roughness also played a role in determining HE sensitivity on a given target. Equation (1) predicts that thermal generation at the target-billet interface should depend on the apparent coefficient of friction and, hence, target roughness. Therefore, a second series of drops was made on quartz targets of varying surface roughness.

Table I lists the five surface finishes that were given to the quartz targets. The apparent coefficients of friction, measured from high-speed photographs of no-go drops, are also listed. Note that surface roughness and apparent coefficient of friction do not correlate monotonically; apparently the Surf-Indicator readings do not uniquely define the surface condition.

The test-billet configuration was changed in this series of drops. The mass of HE was decreased to try to minimize the violence of explosive events and hence to speed the clean-up operation between events. The HE mass was reduced by over-pressing a PBX-9404 cylinder (MT 264, 3.00 in. diam by 2.31 in. high) with inert PBX mockup

TABLE I

SURFACE FINISH AND COEFFICIENT OF FRICTION OF QUARTZ TARGETS

Surface Treatment	Surface Roughness[a] (μin.)	Apparent Coefficient of Friction[b]
Sandblasted with 0.001-in. glass beads	1-2	0.092
Ground with No. 900 grinding powder on grinding wheel	6-7	0.056
Ground with No. 225 grinding powder on grinding wheel	60-80	0.114
Sandblasted with No. 120 grit	180-220	0.151
Sandblasted with No. 20 grit	> 1000	0.243

[a] Average value calculated from all valid no-go drops.

[b] Measured by Cutler-Hammer Surf-Indicator.

in a (MT 840, 6 in. radius) mold. The HE cylinder and over-pressed hemisphere are shown in Fig. 5. The entire assembly was then machined down to a 10-in.-diam hemisphere, leaving an exposed HE pole. The pendulum configuration keeps the billet horizontal, so the PBX sensitive pole, rather than the inert, will strike the target plate. This modification of the skid-test billet can be fabricated with two pressings and one machining operation in sequence, thus speeding up fabrication and reducing cost. No Micarta top plate need be glued to the assembly when the billets are dropped in the pendulum configuration.

IV. RESULTS

Table II summarizes the experimental 50% drop heights and the thermal conductivities of the targets used in the first series of experiments. The experimental 50% drop height for PBX 9404 dropped on the quartz targets was determined by the up-down method of statistical analysis.[8] Because the aluminum oxide targets had two different surface finishes, data were insufficient to permit determination of the 50% drop height by the up-down method.

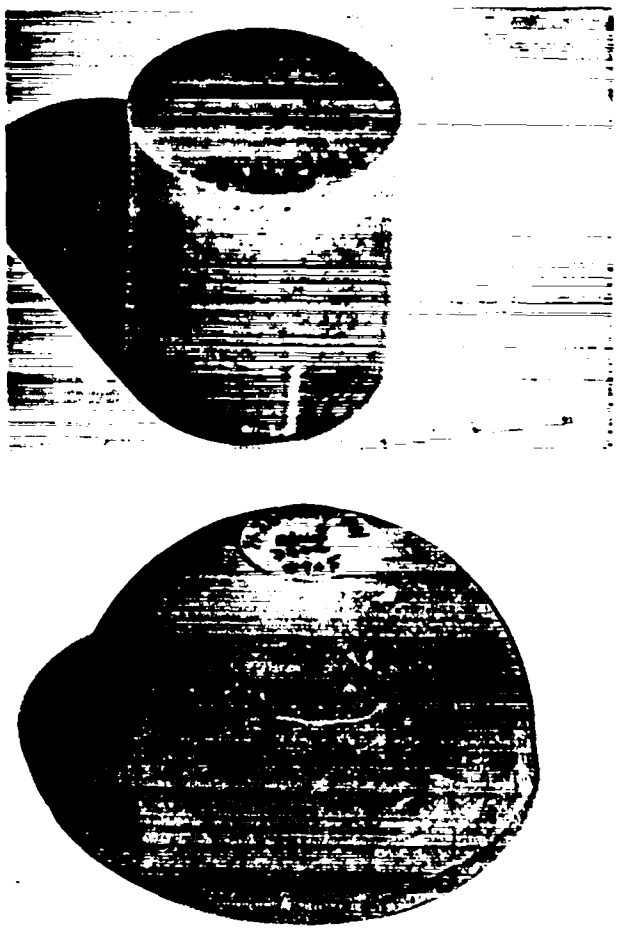

Fig. 5. "Sensitive-pole" drop test billet.

The values given in Table II are estimates based on the available data. Drops from 25, 50, 100, and 150 ft produced no events on the gold targets. Because the drop tower is 150 ft high, no higher drops could be made.

Table III is a summary of the drops onto quartz targets from the first drop series. These data on quartz targets indicate not only a markedly decreased 50% drop height (increased sensitivity), but also a significantly lowered variance for the test.

Table IV is a summary of the drops onto the aluminum oxide targets. In drops 1 through 3, the surface roughness of the targets was 50 to 80 μin.; and in drops 4 through 12, the surface roughness was 20 to 35 μin.

TABLE II

EXPERIMENTAL 50% DROP HEIGHTS

Target Material	Thermal Conductivity (cal/sec-cm-°C)	Experimental Drop Height (ft)
Gold	7.03×10^{-1}	> 150
Aluminum oxide (20- to 35-μ in. surface roughness)	2.10×10^{-2}	~ 19
Aluminum oxide (50- to 80-μ in. surface roughness)	2.10×10^{-2}	~ 11
Quartz	4.05×10^{-3}	1.8

TABLE III

DROPS ON QUARTZ TARGETS

Height (ft)	Drop Number 1	2	3	4	5	6	7	8	9	10
1.5	N		N		N		N		N	
2.12		E		E		E		E		N

N = no event.

E = event.

TABLE IV

DROPS ON ALUMINUM OXIDE TARGETS

Height (ft)	Drop Number 1	2	3	4	5	6	7	8	9	10	11	12
18.5										E		N
15.6							E[a]		N		N	
13.1						N		N				
11.0	E		E		N							
9.25		N		N								

[a] High-speed motion pictures showed drop No. 7 to be invalid.

Table V gives the apparent coefficients of friction for the gold, aluminum oxide, and quartz targets as obtained from analysis of drop films.

The plastic-flow stress for PBX 9404 was determined to be 28,000 lb/in.^{2} and 34,400 lb/in.^{2} for billets in the first and second series, respectively. These values were assumed to be constant over the entire regime of studies and were used in all calculations.

For constant stress and plastic flow, the deformation diameter, corrected for angle of impact, should vary with the 0.25 power of the drop height, as in Eq. (6). The deformation diameter versus drop height, corrected for differing angles, is plotted in Fig. 3 for the first drop series. These data plot on log-log paper with a least-squares slope of 0.25, as indicated by Eq. (6). Thus, the assumption of constant stress and plastic flow seems justified.

Table VI summarizes the various physical and thermal properties used to calculate the critical drop heights expected under the given experimental conditions. Table VII summarizes the thermal-kinetic properties of pure crystalline HMX used in these calculations. These values were obtained from LASL's Group GMX-2.[9] An initial billet temperature of 530°R was used in all calculations.

Table VIII gives the calculated 50% drop heights of PBX 9404 dropped on various targets and the corresponding experimental values for the first series of drops. Table IX contains the apparent coefficient of friction and the experimental and calculated drop heights for the second series of drops of sensitive-pole PBX-9404 billets onto quartz targets with various surface finishes. Figure 6 plots the data of Table IX as experimental or calculated

TABLE V

APPARENT COEFFICIENTS OF FRICTION

Target Material	Apparent Coefficient of Friction
Gold	0.117
Aluminum oxide[a] (20- to 35-μ in. surface roughness)	0.0576
Aluminum oxide[b] (50- to 80-μ in. surface roughness)	0.0808
Quartz	0.132

[a] Average from three "no go" drops.

[b] Average from "no go" drops.

TABLE VI

PHYSICAL AND THERMAL PROPERTIES USED IN CALCULATIONS

Material	Density (g/cm^3)	Heat Capacity (cal/g-°C)	Thermal Conductivity (cal/sec-cm-°C)	Thermal Diffusivity (cm^2/sec)
HMX	1.91	0.295	9.2×10^{-4} [a]	1.65×10^{-3} [b]
Quartz	2.67	0.188	4.05×10^{-3}	8.11×10^{-3}
Aluminum oxide	3.40	0.18	2.1×10^{-2}	3.45×10^{-2}
Gold	19.3	0.0316	7.03×10^{-1}	1.16

[a] No value of thermal conductivity for crystalline HMX was available; this measured value for PBX 9404 was used in all calculations.

[b] Based on thermal conductivity of PBX 9404.

drop height versus coefficient of friction. Corresponding calculated and experimental values on quartz targets from the first series of drops are also shown on this plot.

V. CONCLUSIONS

These two series of drops on controlled target surfaces substantiate the proposed thermal-transport mechanism of initiation in the skid test. The extremely wide range in 50% drop heights on the three different target materials indicates the importance of target thermal conductivity; this is a necessary consequence of the thermal-transport mechanism. Materials with high thermal conductivities are much less likely to produce events when HE is dropped on them than are materials with lower thermal conductivities. During the series of experiments with the gold target, one of the drops from 150 ft missed the target and struck a freshly sand-blasted aluminum surface; no explosion occurred. The thermal conductivity of aluminum is 76% that of gold.

In the first series of drops, excellent agreement was obtained between the critical drop-height calculations and experimental 50% drop heights, where sufficient experimental data could be obtained for comparison. The calculated critical drop height for PBX 9404 on gold targets is out of the range of the LASL skid test; the fact that no events could be produced on gold targets is consistent with these calculations. Insufficient drops were made on the two aluminum oxide surfaces to determine 50% drop heights precisely; however, calculations indicated critical heights close to the estimated 50% heights and also distinguished between the results obtained with the two surface finishes.

TABLE VII

THERMAL-KINETIC PROPERTIES OF HMX USED IN CRITICAL DROP-HEIGHT CALCULATIONS

Property	Value	Units
Heat of reaction (burning)	6.66×10^{5}	cal/(g-mol)
Heat of melting	50	cal/g
Arrhenius frequency factor	5.0×10^{19}	sec^{-1}
Arrhenius activation temperature, E^{+}/R	2.63×10^{4}	°K
Crystal melting temperature	553	°K

TABLE VIII

EXPERIMENTAL AND CALCULATED 50% DROP HEIGHTS

Target Material	Drop Height (ft) Calculated	Experimental
Gold	515	> 150
Aluminum oxide (20- to 35-μin. surface roughness)	22.8	~ 19
Aluminum oxide (50- to 80-μin. surface roughness)	14.2	~ 11
Quartz	1.25	1.8

TABLE IX

COEFFICIENT OF FRICTION, EXPERIMENTAL DROP HEIGHT AND CALCULATED CRITICAL HEIGHT OF PBX-9404 BILLETS ON QUARTZ TARGETS

Coefficient of Friction	Experimental Drop Height (ft)	Calculated Critical Drop Height (ft)
0.056	4.8	3.76
0.092	1.8	1.48
0.114	2.4	1.0
0.151	0.5	0.61
0.243	0.7	0.28

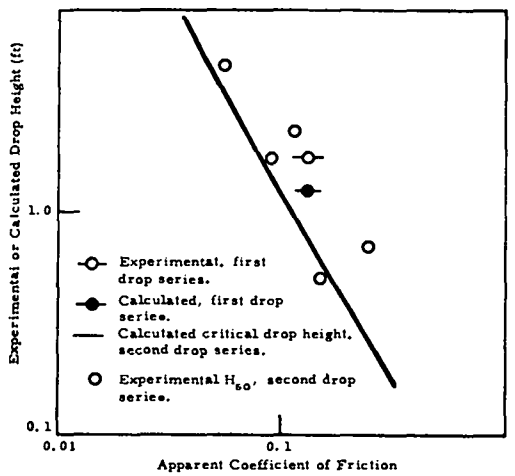

Fig. 6. Effect of target roughness on PBX 9404 drop-test sensitivity on quartz targets.

The second series of drops onto quartz surfaces with various finishes demonstrated the importance of thermal-flux generation at the target-billet interface in sensitizing behavior in the drop test, as well as demonstrating the veracity of the thermal-transport model. Surface roughness is not a unique measure of surface condition; the 1- to 2-μin. surface prepared by blasting with 0.001-in. glass beads appeared quite smooth to the Surf-Indicator, but had a surprisingly high (0.09) coefficient of friction with correspondingly low (1.8 ft) drop height. The apparent coefficient of friction is the most difficult to measure and least reproducible data input in the analysis of the drop test.

In the drop test sensitive-pole billets behave like the more difficult-to-fabricate spherical shell billets used in all previous tests. The higher drop heights, both experimental and calculated, shown in Fig. 6 for the conventional billets, are caused by a lower measured plastic-flow strength (28,000 psi vs 34,000 psi) for these billets. Plastic-flow strength of PBX formulations varies from lot to lot, and must be measured for each series.

There is some indication that drop height goes through a minimum as surface roughness increases, as shown by the last data point in Fig. 6. Such behavior would be expected if machining of the HE occurred and caused the impact energy to be deposited in a finite volume of HE rather than concentrated as a line source at the sliding boundary. In this case, the geometry represented mathematically by the flux-boundary condition would be altered and the thermal-transport model would not be expected to hold.

In summary, this study indicates that the primary mechanism in initiation by oblique impact is thermal generation and transport at the billet-target interface. Factors such as billet stiffness, sliding velocity, and target roughness (up to the limit where machining occurs) affect the generation of the heat at the interface and vary the discrimination capability of the test. Targets of high thermal conductivity transport the heat away from the HE billet, thus desensitizing the test. Sliding velocity (determined by drop height and impact angle), plastic-flow stress (billet stiffness), coefficient of friction (surface finish), and target conductivity are thus the strongest variables affecting skid-test sensitivity. When the experimental drop conditions conform to the idealizations of constant-stress impact and thermal generation at a well-defined target-billet interface, then these calculations quantitatively predict skid-test drop heights within limits of uncertainty of the input data and the experimental drop heights.

ACKNOWLEDGMENTS

The mechanical-impact model developed in this study was based on earlier unpublished work by Charles A. Anderson, Group GMX-3, Los Alamos Scientific Laboratory. We are deeply indebted to Anderson for many discussions concerning the impact model and subsequent heat-transfer calculations.

REFERENCES

1. A. S. Dyer and J. W. Taylor, "Initiation of Detonation by Friction on a High Explosive Charge," The Fifth Symposium on Detonation, Pasadena, California, August 1970.

2. F. P. Bowden and O. A. Gurton, Proc. Roy. Soc. (London) A 198, 337 (1949).

3. A. Yoffe, Proc. Roy. Soc. (London) A 198, 373 (1949).

4. M. J. Furey, Ind. Eng. Chem. 61, 12 (1969).

5. R. Holm, J. Appl. Phys. 19, 361 (1948).

6. J. F. Archard, Wear 2, 438 (1958).

7. J. Zinn and C. L. Mader, J. Appl. Phys. 31, 323 (1960).

8. W. J. Dixon and F. J. Massey, Introduction to Statistical Analysis, McGraw-Hill Co., New York, 1957, pp. 319-327.

9. R. Rogers, LASL Group GMX-2, Private Communication.

KT/sf: 325 (50)